RAA 2021 Vol. **21** No. **2**, 45(8pp) doi: 10.1088/1674-4527/21/2/45

http://www.raa-journal.org *http://iopscience.iop.org/raa*

Research in Astronomy and Astrophysics

Discovery of Four New Clusters in the Cygnus Cloud

Song-Mei Qin (秦松梅)[1], Jing Li (李静)[1,3], Li Chen (陈力)[2,4] and Jing Zhong (钟靖)[2]

[1] Physics and Space Science College, China West Normal University, Nanchong 637000, China; *lijing@bao.ac.cn,chenli@shao.ac.cn,jzhong@shao.ac.cn*

[2] Key Laboratory for Research in Galaxies and Cosmology, Shanghai Astronomical Observatory, Chinese Academy of Sciences, Shanghai 200030, China

[3] Chinese Academy of Sciences South America Center for Astronomy, Beijing 100101, China

[4] School of Astronomy and Space Science, University of Chinese Academy of Sciences, Beijing 100049, China

Received 2020 April 1; accepted 2020 August 11

Abstract We report the discovery of four new open clusters (named QC 1, QC 2, QC 3 and QC 4) in the direction of Cygnus Cloud and select their members based on five astrometric parameters (l, b, ϖ, μ_{α}^{*}, μ_{δ}) of *Gaia* DR2. We also derive their astrophysical parameters for each new cluster. Structure parameters are generated by fitting the radial density distribution with a King's profile. Using solar metallicity, we performed isochrone-fitting on their purified color-magnitude diagrams (CMDs) to derive the age of the clusters. The known cluster NGC 7062 in an adjacent area is chosen to verify our identification process. The estimated distance, reddening and age of NGC 7062 are in good agreement with the literature.

Key words: Galaxy: open clusters and associations — stars: kinematics and dynamics — methods: data analysis

1 INTRODUCTION

Open clusters (OCs), lying close to the Galactic plane, have long been a powerful tool to study the structure and evolution of the Galactic disk (Janes & Adler 1982; Dias & Lépine 2005; Frinchaboy et al. 2013). A majority of stars in the Galactic disk are formed in clusters (Lada & Lada 2003). Although many clusters were dissolved by dynamical disruption processes, the surviving OCs have large age and distance range and can be relatively accurately dated. The spatial distribution and kinematic properties of OCs provide critical constraints on the overall structure and dynamical evolution of the Galactic disk, meanwhile, their [Fe/H] values serve as excellent tracers for the abundance gradient along the Galactic disk, as well as many other important disk properties, such as the age-metallicity relation, abundance gradient evolution, etc (Chen et al. 2003; Jacobson et al. 2016).

Most OCs are located in the Galactic disk. Kharchenko et al. (2013) listed 3006 star clusters, including about 2700 OCs, most of which were located within 3 kpc of the Sun. By extrapolating the solar vicinity to the whole disk, about 10^5 OCs are thought to exist (Piskunov et al. 2006). Most recently, utilizing *Gaia* Data Release 2 (DR2) alone, Cantat-Gaudin & Anders (2020) investigated a list of thousands of clusters from the literature, and homogeneously derived kinematic and distance parameters for 1481 confirmed clusters, in the meantime revealing that some of the clusters from the literature are probably not real clusters. By systematically scanning along the Galactic disk with *Gaia* DR2, Castro-Ginard et al. (2020) detected 582 previously unknown OCs.

Stars in an OC form simultaneously with collapsing molecular clouds (see reviews by Lada & Lada 2003; Portegies Zwart et al. 2010), hence sharing various properties. By assuming that OC member stars are co-moving, the vector point diagram (VPD) will exhibit a clustering of member stars within the more dispersed field star distribution. Moreover, since they are coeval and located at nearly the same distance, the member stars are expected to show a relatively narrow main-sequence feature on the color-magnitude diagram (CMD). Reliably identifying cluster member stars is extremely important and completely necessary for the studies of OCs, however, the actual reliability of member stars selected by using the astrometric and/or photometric criteria greatly depends on the observational precision. The ambitious European Space Agency (ESA) mission *Gaia* [1] conducted

[1] `https://www.cosmos.esa.int/gaia`

an all-sky survey, which has made its second data release available (*Gaia* DR2; Gaia Collaboration et al. 2016, 2018) providing five precise astrometric parameters (l, b, ϖ, μ_α^*, μ_δ) and three band photometry (G, G_{BP} and G_{RP}) for more than one billion stars (Lindegren et al. 2018). This allows us to investigate a large number of OCs with unprecedented accuracy.

The Cygnus Cloud area, usually accepted to be part of the Local Arm seen tangentially, at a relative proximity of 1–2 kpc with numerous young OCs and HII regions, is a typical star-forming area. It is also a rather complex area including a concentration of dust clouds with heavy and non-uniform absorption and reddening, which leads to the possibility of missing some star clusters in the area. Analyzing the region of Cygnus Cloud with *Gaia* DR2 data, we have noticed the existence of four clusters unreported in the literature to our best knowledge. Figure 1 is an AllWISE-W3 image around the Cygnus Cloud, in a $15^\circ \times 7.5^\circ$ size, centered at about $l = 83.76^\circ$, $b = 0.55^\circ$. WISE[2] is a NASA Medium Class Explorer mission that scanned the sky methodically in the 3.4 μm, 4.6 μm, 12 μm and 22 μm mid-infrared bandpasses (W1, W2, W3 and W4) in 2010 and 2011 (Wright et al. 2010) and the AllWISE program extends the work of the successful WISE by combining data from the cryogenic and post-cryogenic survey phases to form the most comprehensive view of the mid-infrared sky currently available. Overlapped on the image we display the spatial distribution of the centers of our newly found OCs, together with the OCs listed by Kharchenko et al. (2013) and Cantat-Gaudin & Anders (2020) located in that area, including the well-defined cluster NGC 7062 as a comparison object.

In this paper, based on precise *Gaia* DR2 astrometry and photometry data, we confirm the true existence of these four new OCs (hereafter named QC 1 through QC 4). In Section 2, we present the data considered in this work and sample reduction process. In Section 3, we describe the detection of the new OCs, including the identification and characterization of the clusters. A discussion about this work is given in Section 4.

2 DATA

When trying to dig up *Gaia* DR2 in nearby molecular clouds, we serendipitously noticed the existence of four new clusters in the Cygnus Cloud. Thanks to *Gaia* DR2, for each of the four new candidate clusters and NGC 7062, we retrieved the positions (l and b), parallaxes (ϖ), proper motions (μ_α^*[3], μ_δ), magnitudes in three photometric filters (G, G_{BP} and G_{RP}) and their associated uncertainties, in an area with a radius of 0.75° centered on the approximate central position. The total numbers of retrieved stars in each of the targeted areas range from 1.3×10^5 to 3.5×10^5. The typical proper motion uncertainty goes from 0.20 mas yr^{-1} for $G \approx 17$ mag, up to 1.2 mas yr^{-1} for $G = 20$ mag. The corresponding parallax (ϖ) uncertainty goes from 0.1 mas at $G \approx 17$ mag, up to 0.7 mas at $G = 20$ mag.

Our target clusters are immersed in a dense star field. It is hard to contrast the cluster members with the background. The most efficient way of hunting for new clusters is to look for clusterings of stars in the velocity space (i.e. the VPD), since OC members have distinctive movement as compared to field stars. For highlighting cluster members in the proper motion distribution diagram, we limited our working sample to magnitude $G < 17$ mag, corresponding to typical astrometric uncertainties of 0.2 mas yr^{-1} in proper motion and 0.1 mas in parallax. In order to further clean our sample, we applied re-normalized unit weight error ($RUWE$) < 1.4 as a criterion for selecting sources with “good” astrometry, following Lindegren (2018). This cut seeks to filter out sources with spurious parallaxes or proper motions and retains about 90% of each cluster sample. Then, we kept the member stars with relative error of parallax $\varpi\_err/\varpi < 15\%$. The above selection clearly revealed the over-density features of our new cluster candidates as well as the known target NGC 7062 in the proper motion distribution diagram as illustrated in Figure 2.

3 ANALYSIS AND RESULTS

3.1 Identification of the New Clusters

To verify the existence of the new clusters by checking the effectiveness of the identification process, we took NGC 7062 as an example and carried out the following steps.

We define different proper-motion boxes to contain each of the five co-moving structures (including NGC 7062) to look for members in terms of spatial coordinates (i.e., in RA and DEC, l and b). The different proper-motion boxes for different clusters are featured in Figure 2, which were set big enough to isolate the proper motion clump but small enough to mitigate the dispersed field star distribution or other adjacent clumping structures in the proper motion distribution diagram.

Subsequently, for stars in each of the proper-motion boxes, the average proper motion distribution (μ_α^*, $\sigma_{\mu_\alpha^*}$; μ_δ, σ_{μ_δ}) of candidate members can be acquired by Gaussian-fitting in corresponding directions. In proper motion space, we then defined a circular region centered on the expected average proper motion with radius $\sigma_\mu =$

[2] *https://www.nasa.gov/mission_pages/WISE/main/index.html*

[3] Here $\mu_\alpha^* = \mu_\alpha \cos\delta$

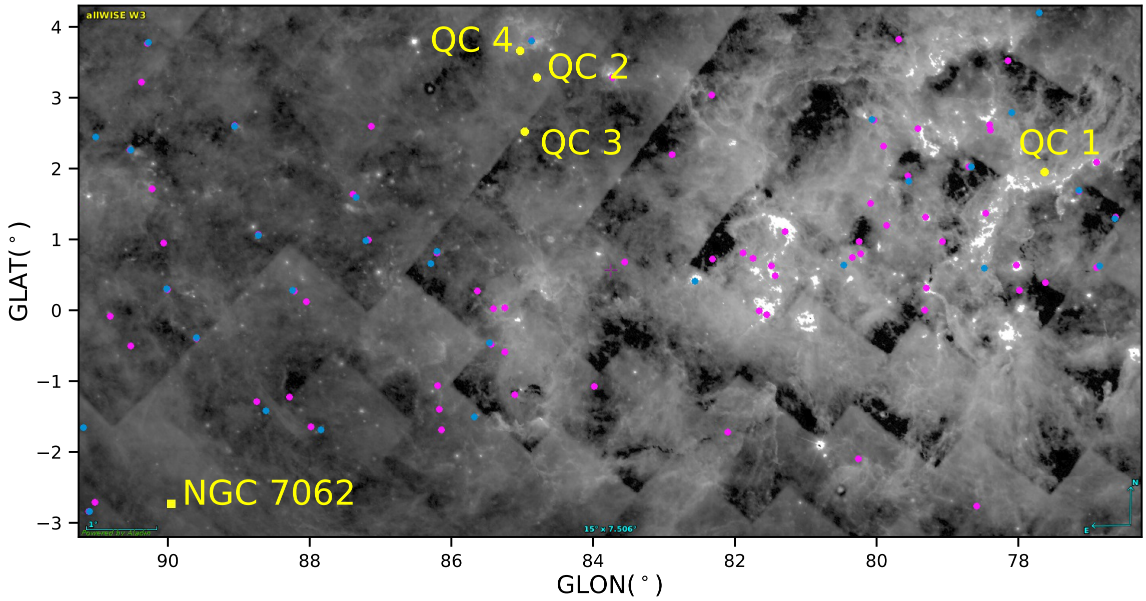

Fig. 1 The AllWISE-W3 image taken from the Aladin server within a $15° \times 7.5°$ size, centered at about $l = 83.76°$, $b = 0.55°$. North is up, east is left. It shows the spatial distribution of our newly found OCs (yellow dots: from QC 1 to QC 4) together with the OCs listed by Kharchenko et al. (2013) (*pink dots*) and Cantat-Gaudin & Anders (2020) (*blue dots*) in the Galactic maps. The single yellow square at the bottom-left is the known cluster NGC 7062.

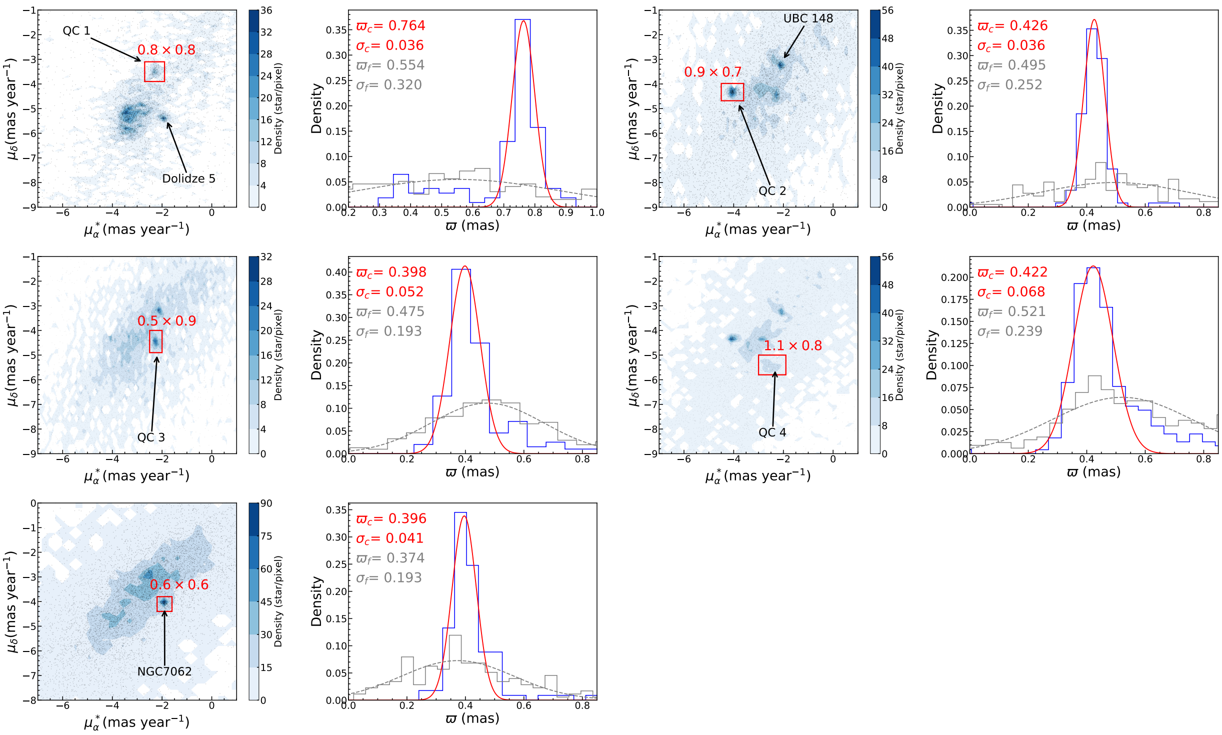

Fig. 2 The proper motion distribution and Gaussian fitting of parallax (ϖ) for four new clusters and NGC 7062. Proper motion distribution: The over-density of each cluster can be clearly seen and the red rectangles indicate initial proper-motion from selecting boxes for each cluster; the color bar on the right represents the number density scale. Gaussian fitting of parallax (ϖ): The blue histogram and red line are for stars selected by proper motion criterion, the grey histogram and dashed line for the field stars selected randomly from the rest of the stars; and the mean value and standard deviation for candidate members (ϖ_c, σ_c) and field stars (ϖ_f, σ_f) are shown at the top left.

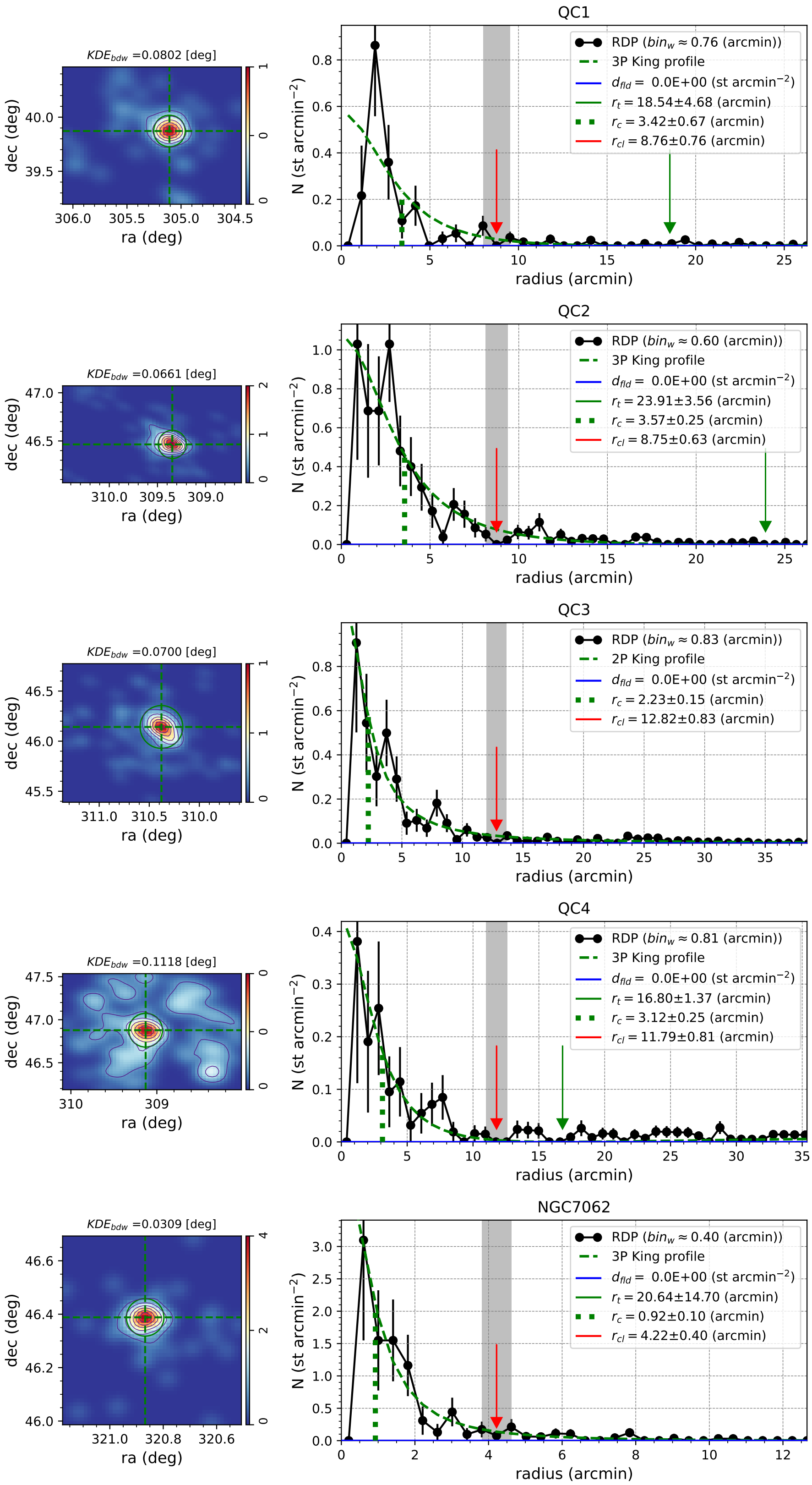

Fig. 3 (QC 1, QC 2, QC 3, QC 4, NGC 7062, from top to bottom respectively) *Left panels*: center determination via a 2D KDE. *Right panels*: radial density profile, black dots are the radial density values in each annulus bin; the horizontal blue line is the field density value $d_{\rm field}$; the red arrow marks the cluster radius with uncertainty region shaded as a gray area; a King profile fit is indicated with the green dashed curve and a vertical green dotted line signifies the $r_{\rm c}$ value.

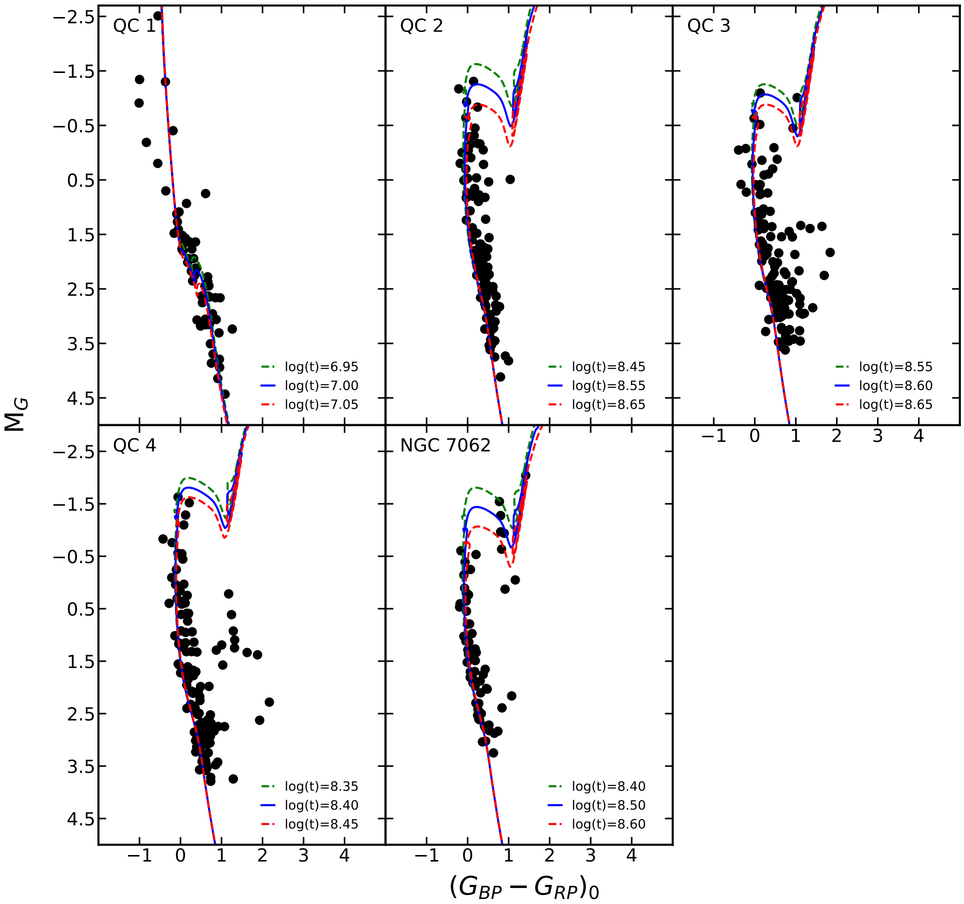

Fig. 4 The CMDs of four new clusters and NGC 7062. Black dots represent member stars from the proper motion and parallax selection. Blue solid lines indicate the best-fitting isochrone while green and red dashed lines signify the possible range of age uncertainties The three isochrones applied the same solar metallicity ($Z_\odot = 0.0152$). Ages are written in the panels for each cluster.

Table 1 The Parameters of Newly Found OCs and NGC 7062 Sorted by Increasing l

Name	N	RA (°)	DEC (°)	l (°)	b (°)	μ_α^* (mas yr^{-1})	μ_δ (mas yr^{-1})	ϖ (mas)	Dist pc
QC 1	72	305.106	39.871	77.635	1.932	-2.30±0.09	-3.48±0.12	0.766±0.02	1261
QC 2	114	309.349	46.469	84.802	3.278	-4.05±0.06	-4.32±0.06	0.424±0.03	2223
QC 3	124	310.381	46.142	84.976	2.513	-2.25±0.10	-4.46±0.13	0.400±0.03	2340
QC 4	130	309.117	46.882	85.036	3.654	-2.51±0.24	-5.43±0.17	0.424±0.04	2230
NGC 7062	67	320.863	46.384	89.963	-2.744	-1.91±0.07	-4.05±0.07	0.395±0.02	2359
NGC 7062[a]	82[b]	320.862	46.385	89.963	-2.743	-1.91±0.13	-4.05±0.09	0.398	2343

All member stars here are brighter than $G = 17$ mag. ^{a}: Parameters available from Cantat-Gaudin & Anders (2020); ^{b}: The number here is from Cantat-Gaudin & Anders (2020) and 82 refers to the cluster star members ($G < 17$ mag, relative error of parallax < 0.15, membership probability > 0.6) of NGC 7062.

$\sqrt{\sigma^2_{\mu^*_\alpha} + \sigma^2_{\mu_\delta}}$ as the kinematic membership criterion for each candidate cluster.

For the remaining candidate member stars, their parallax distribution exhibits a prominent peak that can be fitted by a Gaussian profile, as the corresponding histograms (blue) and fitting lines (red) signify in Figure 2; the gray histograms and dashed lines refer to the same number of field stars selected randomly in position space from all stars except for those contained in the proper-motion box; the fitted parallax values and standard deviations for cluster candidate members (ϖ_c, σ_c) and field stars (ϖ_f, σ_f) are marked in the panels. We then excluded stars with parallax (ϖ) ranging out of one sigma (σ_ϖ) from the Gaussian distribution peak to further purify the member star samples.

In summary, in the identification process for the four new OC candidates as well as the comparison cluster NGC 7062, the final sample of member stars for each

Table 2 The Structure Parameters of Newly Found OCs and NGC 7062

Name	r_c (arcmin)	r_t (arcmin)	r_{cl} (arcmin)
QC 1	3.42	18.54	8.76
QC 2	3.57	23.91	8.75
QC 3	2.23	–	12.82
QC 4	3.12	16.80	11.79
NGC 7062	0.92	20.64	4.22

cluster possesses the following features: (i) the proper motion distribution shows a distinct over-density in the corresponding VPD; (ii) the parallax distribution manifests an apparent peak, while the projected spatial distribution exhibits certain central concentration (see the left panels of Fig. 3); and (iii) the selected members in the CMD reveal a relatively narrow main sequence (see in Fig. 4).

3.2 Radial Density Profile

We apply Automated Stellar Cluster Analysis (ASteCA[4]) code (Perren et al. 2015) to determine the cluster center or maximum spatial density point through a two-dimensional (2D) Gaussian kernel density estimator (KDE) fitted on the position space. The spatial distributions of each cluster's member stars that satisfy the above selection criteria are also displayed in Figure 3 (left panels), which reveal the spatial concentration feature. However, the aggregate structures of some clusters (such as QC 1 and QC 4) are relatively sparse, as can be seen from the radial density profiles (RDPs) which are also generated with ASteCA.

The "cluster radius" $r_{\rm cl}$ employs the value where the radial density profile stabilizes around the field density value ($d_{\rm field}$), which is identical to the "limiting radius" $R_{\rm lim}$ defined in Bonatto & Bica (2005). ASteCA searches the $r_{\rm cl}$ by implementing several tolerance thresholds to define when the "stable" condition is met. The RDP is obtained by generating concentric square rings via an underlying 2D histogram/grid in the positional space. The first RDP point is calculated by counting the number of stars in the first square ring with a radius of half the bin width, divided by the area of the cell. The calculus process is repeated to get the second RDP point (second square ring, radius of 1.5 bin width), third RDP point (third square ring, radius of 2.5 bin width)... until 75% of the length of the frame is reached. Also, the RDP function could mask a bad pixel to correctly avoid empty regions. For each cluster, ASteCA first attempts a three-parameter fit to the RDP and, if that is not possible because of either no convergence or an unrealistic $r_{\rm t}$, falls back on the two-parameter fit (King 1962, 1966; Perren et al. 2015)

$$f(r) = f_b + f(0)/[(\frac{1}{\sqrt{1+(\frac{r}{r_c})^2}} - \frac{1}{\sqrt{1+(\frac{r_t}{r_c})^2}})^2] \quad (1)$$

or

$$f(r) = f_b + f(0)/[1+(r/r_c)^2] \quad (2)$$

where $r_{\rm t}$ means tidal radius, $r_{\rm c}$ means core radius and $f(r)$ is the surface number density. The fitting results are featured in Figure 3 (right panels).

For each of the four new clusters and NGC 7062, the number of selected member stars, the cluster central positions (in RA and DEC, l and b) determined from Gaussian KDE, the mean value and standard deviation of proper motion and parallax found by fitting the Gaussian distribution function are listed in Table 1; the structure parameters $r_{\rm t}$, $r_{\rm c}$ and $r_{\rm cl}$ obtained by ASteCA are expressed in Table 2.

3.3 Isochrone Fittings

The CMDs of each cluster were drawn with *Gaia* photometry, as depicted in Figure 4, and the black dots refer to the member stars selected by the criteria in Section 3.1. We also perform a visual fitting process to make an initial estimate for the age parameter of the new OCs.

To determine the age parameter of the newly discovered clusters and NGC 7062, we retrieved the Padova isochrones (Marigo et al. 2017) with solar metallicity $Z_\odot$ = 0.0152 (Caffau et al. 2009, 2011) and *Gaia* photometric system (Evans et al. 2018) from CMD 3.3[5], and the logarithm of ages varies in a range of 6.60 to 10.10 with an interval of 0.05. We acquired the reddening values of all the member stars from the Stilism[6] three-dimensional (3D) dustmaps and the distance from the catalog of 1.33 billion stars in *Gaia* DR2 provided by Bailer-Jones et al. (2018), and we use the ratios $A_G = 2.74 \times E(B-V)$ and $E(BP-RP) = 1.339 \times E(B-V)$ (Casagrande & VandenBerg 2018; Zhong et al. 2019) in calculating the extinction values. Consequently, we performed an eye-fitting procedure to find the most appropriate isochrone on the observed CMD by shifting in a reasonable range of age parameters.

We carefully inspected the match of the isochrones to the key evolutionary regions, such as the upper main sequence, the turn-off point and the red giant or red clump features on the CMDs. By shifting the isochrones to best fit the CMD of the member stars, we obtained the age

[4] https://asteca.readthedocs.io/en/latest/about.html

[5] http://stev.oapd.inaf.it/cgi-bin/cmd/

[6] https://stilism.obspm.fr/

Table 3 The Parameters of Newly Found OCs and NGC 7062

Name	$E(B-V)$ mag	$m-M$ mag	log(t)
QC 1	0.756±0.280	12.55	7.00
QC 2	0.552±0.010	13.24	8.55
QC 3	0.577±0.019	13.42	8.60
QC 4	0.556±0.049	13.26	8.40
NGC 7062	0.580±0.051	13.45	8.50
NGC 7062	–	–	8.84[a]

[a]The age parameter here is from Kharchenko et al. (2013).

of each cluster. Figure 4 shows the fitting result for four new clusters and NGC 7062, the blue solid line is our adopted best-fitting isochrone, and green and red dashed lines signify the possible range of age uncertainties. The astrophysical parameters such as reddening ($E(B-V)$), distance modulus ($m-M$) and age (log(t)) of the four new clusters and NGC 7062 are listed in Table 3.

4 DISCUSSION

Based on the reliable *Gaia* DR2 data, we have identified four new OCs named QC 1, QC 2, QC 3 and QC 4 in the east part of the Cygnus Cloud region ($77° \leq l \leq 90°$ and $-3° \leq b \leq 4°$). We performed a field star decontamination process based on precise *Gaia* astrometric data. The selected member stars of these new clusters show apparent proper motion over-density in the corresponding VPD, relatively central concentration in the 3D spatial distribution and a clear main sequence feature on the CMD. For each cluster, we use solar metallicity, the averaged distance values from *Gaia* DR2 (Bailer-Jones et al. 2018) and the reddenings from Stilism 3D dustmaps for all individual member stars. Then we performed an eye-fitting procedure to find the most appropriate isochrone on the observed CMD by shifting the age parameter in a reasonable range.

For testing and verifying our member selection and isochrone fitting procedure, we take NGC 7062 as a comparison cluster to go through the same filtering and analysis processes. As for NGC 7062, we analyzed the *Gaia* DR2 data in a field of 0.75 deg radius around its center at l = 89.963°, b = −2.744°. Finally, we obtained 67 member stars brighter than G = 17 mag, of which 47 stars are common to Cantat-Gaudin & Anders (2020)'s sample (including 82 member stars in total with $G <$ 17 mag, relative error of parallax $<$ 0.15 and probability $>$ 0.7). The final mean distance (2334 pc) is quite consistent with that from Cantat-Gaudin & Anders (2020) (Dist = 2343 pc); the mean value of $E(B-V) \approx 0.582$ for NGC 7062 is larger than the value (0.46) of Peniche et al. (1990) and the value (0.32) of Güneş et al. (2012), both of which are derived from visual isochrone-fitting. The age of NGC 7062 in our work (log(t) = 8.50) is a bit older than that (log(t) = 8.45) of Peniche et al. (1990), but a bit younger than the age (log(t) = 8.84) of Kharchenko et al. (2013) and the age (log(t) = 9.0) of Güneş et al. (2012). Our properties for NGC 7062 are in good agreement with those inferred from Cantat-Gaudin & Anders (2020), which are also based on *Gaia* DR2 data.

In addition, when submitting this paper we found out that in Liu & Pang (2019)'s newly published paper, two clusters listed in their catalog (Nr.600, Nr.506) have nearly the same positions as our QC 2 and QC 3, respectively. In their work results, these two objects are estimated to be very young (4–5 Myr) and categorized as Class 3 candidates that need further confirmation. For our four new clusters, more future observations are needed to further investigate their properties. In particular, more spectroscopic data for the member stars will be of prime importance to determine the dynamical and chemical nature of these clusters.

Acknowledgements We thank the anonymous referee for constructive comments that significantly improved the quality of the paper. This work is supported by the National Natural Science Foundation of China (NSFC) under Grant No. 11703019 and China West Normal University Grants 17C053, 17YC507 and 16E018. L.C. acknowledges support from NSFC under Grant No. 11661161016. J.Z. would like to acknowledge the NSFC under Grant No. U1731129.

This work has made use of data from the European Space Agency (ESA) mission *Gaia* (`https://www.cosmos.esa.int/gaia`), processed by the *Gaia* Data Processing and Analysis Consortium (DPAC, `https://www.cosmos.esa.int/web/gaia/dpac/consortium`). Funding for the DPAC has been provided by national institutions, in particular the institutions participating in the *Gaia* Multilateral Agreement.

References

Bailer-Jones, C. A. L., Rybizki, J., Fouesneau, M., Mantelet, G., & Andrae, R. 2018, AJ, 156, 58
Bonatto, C., & Bica, E. 2005, A&A, 437, 483
Caffau, E., Ludwig, H. G., Steffen, M., Freytag, B., & Bonifacio, P. 2011, Sol. Phys., 268, 255
Caffau, E., Maiorca, E., Bonifacio, P., et al. 2009, A&A, 498, 877
Cantat-Gaudin, T., & Anders, F. 2020, A&A, 633, A99
Casagrande, L., & VandenBerg, D. A. 2018, MNRAS, 479, L102
Castro-Ginard, A., Jordi, C., Luri, X., et al. 2020, A&A, 635, A45
Chen, L., Hou, J. L., & Wang, J. J. 2003, AJ, 125, 1397
Dias, W. S., & Lépine, J. R. D. 2005, ApJ, 629, 825

Evans, D. W., Riello, M., De Angeli, F., et al. 2018, A&A, 616, A4
Frinchaboy, P. M., Thompson, B., Jackson, K. M., et al. 2013, ApJL, 777, L1
Gaia Collaboration, Prusti, T., de Bruijne, J. H. J., et al. 2016, A&A, 595, A1
Gaia Collaboration, Brown, A. G. A., Vallenari, A., et al. 2018, A&A, 616, A1
Güneş, O., Karataş, Y., & Bonatto, C. 2012, New Astron., 17, 720
Jacobson, H. R., Friel, E. D., Jílková, L., et al. 2016, A&A, 591, A37
Janes, K., & Adler, D. 1982, ApJS, 49, 425
Kharchenko, N. V., Piskunov, A. E., Schilbach, E., Röser, S., & Scholz, R. D. 2013, A&A, 558, A53
King, I. 1962, AJ, 67, 471
King, I. R. 1966, AJ, 71, 276
Lada, C. J., & Lada, E. A. 2003, ARA&A, 41, 57
Lindegren, L. 2018, Re-normalising the Astrometric chi-square in Gaia DR2, Technical Note, Lund Observatory, gAIA-C3-TN-LU-LL-124
Lindegren, L., Hernández, J., Bombrun, A., et al. 2018, A&A, 616, A2
Liu, L., & Pang, X. 2019, ApJS, 245, 32
Marigo, P., Girardi, L., Bressan, A., et al. 2017, ApJ, 835, 77
Peniche, R., Pena, J. H., & Diaz, S. 1990, in Astrophysical Ages and Dating Methods, eds. E. Vangioni-Flam, M. Casse, J. Audouze, & J. Tran Thanh Van, 141
Perren, G. I., Vázquez, R. A., & Piatti, A. E. 2015, A&A, 576, A6
Piskunov, A. E., Kharchenko, N. V., Röser, S., Schilbach, E., & Scholz, R. D. 2006, A&A, 445, 545
Portegies Zwart, S. F., McMillan, S. L. W., & Gieles, M. 2010, ARA&A, 48, 431
Wright, E. L., Eisenhardt, P. R. M., Mainzer, A. K., et al. 2010, AJ, 140, 1868
Zhong, J., Chen, L., Kouwenhoven, M. B. N., et al. 2019, A&A, 624, A34